IOPscience iopscience.iop.org

Home Search Collections Journals About Contact us My IOPscience

The role of an electronic surface state in the stopping power of a swift charged particle in front of a metal

This article has been downloaded from IOPscience. Please scroll down to see the full text article.

2008 J. Phys.: Condens. Matter 20 304209

(http://iopscience.iop.org/0953-8984/20/30/304209)

View the table of contents for this issue, or go to the journal homepage for more

Download details:
IP Address: 129.252.86.83
The article was downloaded on 29/05/2010 at 13:36

Please note that terms and conditions apply.

J. Phys.: Condens. Matter **20** (2008) 304209 (7pp) doi:10.1088/0953-8984/20/30/304209

# The role of an electronic surface state in the stopping power of a swift charged particle in front of a metal

**V M Silkin[1], M Alducin[2], J I Juaristi[2], E V Chulkov[1,2] and P M Echenique[1,2]**

[1] Donostia International Physics Center (DIPC), Paseo de Manuel Lardizabal 4, 20018 San Sebastián, Basque Country, Spain
[2] Departamento de Física de Materiales, Facultad de Ciencias Químicas, Universidad del País Vasco (UPV/EHU) and Centro de Física de Materiales, Centro Mixto CSIC-UPV/EHU, Apartado 1072, 20080 San Sebastián, Basque Country, Spain

E-mail: waxslavs@sc.ehu.es

Received 20 December 2007, in final form 26 February 2008
Published 8 July 2008
Online at stacks.iop.org/JPhysCM/20/304209

**Abstract**

We study the stopping power and friction coefficient of a slow charged particle moving parallel to noble metal (111) surfaces. In the description of the surface electronic structure, information about a wide energy gap at the surface Brillouin zone, at the Fermi level, and the partly occupied s–$p_z$ surface state is introduced via the use of a model potential. The stopping power, $S(b, v)$, and friction coefficient, $\gamma(b, v)$, versus the projectile velocity $v$ and its distance from the surface $b$ are investigated within linear response theory with self-consistent evaluation of the surface response function. The present calculations demonstrate the striking differences in the behavior of $S(b, v)$ and $\gamma(b, v)$ in comparison with those obtained from simpler models. In particular, for very low velocities, $S(b, v)$ and $\gamma(b, v)$ decay as $b^{-3}$ at large $b$, mainly due to the electron–hole excitations within the surface state, instead of the $\sim b^{-4}$ behavior expected from a jellium model. For velocities close to the surface state Fermi velocity, $v_F^{SS}$, the energy losses with characteristic $\sim b^{-2}$ decay are dominated by the excitation of the acoustic surface plasmons that can exist at some surfaces with partly occupied surface states.

(Some figures in this article are in colour only in the electronic version)

## 1. Introduction

The study of the energy loss of ions interacting with metal surfaces has been an active field of research for many years [1]. Various experiments have provided information about the energy losses experienced by protons [2–4] and heavy ion projectiles [5–7] under grazing scattering conditions. In the analysis of results of these experiments, a central quantity is the so-called distance dependent stopping power, i.e. the energy lost per unit path length by the ion traveling parallel to the metal surface, as a function of the ion surface separation. Echenique and Pendry [8] used a local response function to calculate this quantity and applied it to the calculation of the energy losses of fast electrons traveling parallel to a planar surface. The applicability of the local response approach was extended to different geometries when it was shown to provide a powerful method to obtain all the multipole contributions to the energy loss probability for electrons interacting with dielectric spheres [9].

In later works, in order to extend the validity of the calculations to lower projectile velocities, wavevector dependent surface dielectric functions were used [10–15]. These calculations were based on the specular reflection model [16, 17]. This model allows us to obtain the surface response function in terms of the bulk response function. The approximation used in the specular reflection model assumes that the conduction electrons are confined by an infinite potential barrier at the surface, and the quantum interference between the outgoing and ingoing components of the electrons reflected at this barrier is neglected. In a different

 © 2008 IOP Publishing Ltd Printed in the UK

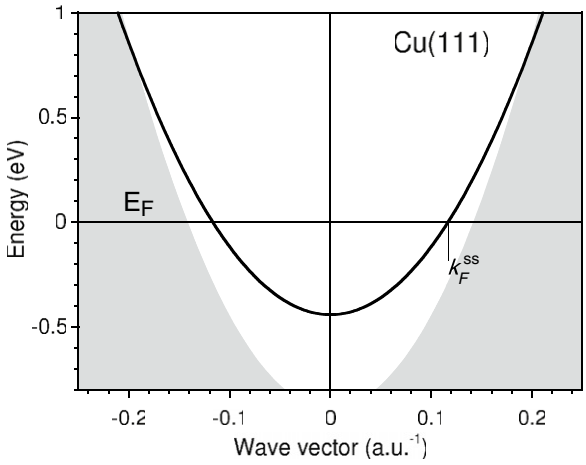


**Figure 1.** Electronic structure of the Cu(111) surface around the surface Brillouin zone center. A parabolic-like surface state dispersion with experimental effective mass $m^*_{SS} = 0.42m_e$ and binding energy $E_{SS} = 0.44$ eV is shown by a thick solid line. The gray area represents the projected bulk electronic states. The energies are relative to the Fermi level shown by the thin horizontal line.

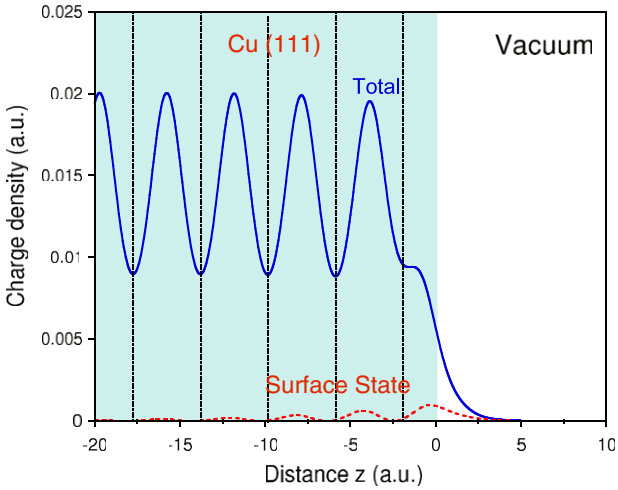


**Figure 2.** Total (solid line) and surface state (dashed line) charge density at the Cu(111) surface as obtained with the use of a model potential of [32]. The colored area corresponds to the solid and the vacuum is on the right side. The vertical dotted lines show the atomic plane positions.

approach, Gravielle and collaborators [18, 19] studied the interaction of a charged particle with the conduction electrons bounded by a finite step potential at the surface. This model describes single particle excitations (electron–hole creation) but does not include collective excitations (plasmons). More recently [20–23], the distance dependent stopping power has been obtained from calculations in which the Kohn–Sham formulation of the density functional theory was used to calculate self-consistently a finite and smooth surface potential barrier. In these works, the jellium model was used to describe the conduction band of the metal; the ionic background made up of nuclei and core electrons was replaced by a uniform positive charge distribution. In [20, 21] the Kohn–Sham orbitals were used to construct the response function of the system in the random phase approximation [24, 25]. In [22, 23] exchange and correlation effects were also included in the calculation of the response within the so-called adiabatic local density approximation [26]. Nevertheless, it was observed that the stopping power for a particle traveling parallel to a metal surface was almost insensitive to this correction. On the contrary, the use of a self-consistently calculated finite surface barrier improved significantly the results obtained within the specular reflection model, for both the stopping power and the total energy loss, up to velocities of the order of $v = 2$–$3v_0$ ($v_0$ is the Bohr velocity) [20, 21]. At higher velocities, the specular reflection model showed to be a reliable approximation.

Finally, for a more realistic description of the energy loss of charged particles moving near metal surfaces [27–31], the Kohn–Sham potential used in the self-consistent jellium calculations [20–23] has been replaced by a realistic model potential [32, 33] that reproduces the width and position of the surface band gap, the energies of the surface state, and the first image state of the metal under study. For the Cu(111) surface and projectile velocities $v > v_0$, it was shown that although this surface exhibits a wide band gap around the Fermi level and a well-defined Shockley surface state the energy loss expected from this model does not differ significantly from its jellium counterpart. This is due to the fact that the presence of the surface state compensates for the reduction of the energy loss due to the band gap [27, 28]. However, recently it has been demonstrated that, due to its two-dimensional character, these surface states can strongly modify the dielectric properties of metal surfaces [31], where the behavior of the friction coefficient for a very slowly moving ion in front of the surface has been investigated. Thus the stopping power of the Cu(111) surface scales as $b^{-3}$, in contrast to the known $b^{-4}$ scaling for electron–hole excitations in a jellium surface [10], where $b$ is the projectile–surface distance.

Here we extend the calculations to higher velocities (keeping the projectile velocity below the Bohr value) to investigate the effect of the acoustic surface plasmon on the energy loss for surfaces with partly occupied surface states [34]. The (111) surfaces of noble metals Cu, Ag, and Au are precisely known to support a partially occupied electron band of the Shockley surface state at the surface Brillouin zone center, $\overline{\Gamma}$ [35–37]. This state has a parabolic-like dispersion with two-dimensional momentum $\overline{\mathbf{k}}$ parallel to the surface and its wavefunction is strongly localized near the surface (see figure 1 for the Cu(111) surface case). Therefore, it forms a quasi-two-dimensional surface state band with a Fermi energy, $E_F^{SS}$, equal to the surface state binding energy at the $\overline{\Gamma}$ point. This surface state is immersed in the sea of bulk electrons and the charge corresponding to the surface state constitutes only a small fraction of the total electronic charge at the metal surfaces, as seen in figure 2. It is this coexistence of such a surface state with bulk electrons at some metal surfaces that can lead to the appearance of these novel collective electronic oscillations, called acoustic surface plasmons [34].

## 2. Theory

The stopping power $S(b, \upsilon)$ of a particle with charge $Z_1$ moving, at a distance $b$, parallel to a metal surface with velocity $\upsilon$ can be expressed as [22, 28]

$$S(b,\upsilon) = \frac{2Z_1^2}{\upsilon}\int \frac{\mathrm{d}\overline{\mathbf{q}}}{(2\pi)^2}\int_0^\infty \mathrm{d}\omega\,\omega\,\mathrm{Im}[W(b,b,\overline{q},\omega)] \times \delta(\omega-\overline{q}\upsilon), \quad (1)$$

where $W(b, b, \overline{q}, \omega)$ is the dynamical screened Coulomb interaction, $\overline{\mathbf{q}}$ is a two-dimensional vector along the surface and $\overline{q} \equiv |\overline{\mathbf{q}}|$. We assume translational invariance of the potential and valence charge density along the surface of the target. At low velocity one can define a distance dependent friction coefficient $\gamma(b) = S(b, \upsilon)/\upsilon$. Normally it is independent of the projectile velocity. Nevertheless, as it will be shown below, this coefficient can also be velocity dependent even for projectile velocities significantly smaller than the Fermi velocity of the target electron system. In the case of a charged particle traveling at large distances $b$ from the metal surface, equation (1) takes the form

$$S(b,\upsilon) = \frac{2Z_1^2}{\pi\upsilon^2}\int_0^\infty \mathrm{d}\overline{q}\,\mathrm{e}^{-2\overline{q}b}\int_0^{\overline{q}\upsilon}\mathrm{d}\omega\,\frac{\omega}{\sqrt{(\overline{q}\upsilon)^2-\omega^2}} \times \mathrm{Im}[g(\overline{q},\omega)], \quad (2)$$

where the surface response function $g(\overline{q}, \omega)$ is expressed in terms of the density–density response function $\chi(z, z', \overline{q}, \omega)$ [38]

$$g(\overline{q},\omega) = -\frac{2\pi}{\overline{q}}\int \mathrm{d}z\int \mathrm{d}z'\,\mathrm{e}^{-\overline{q}(z+z')}\chi(z,z',\overline{q},\omega). \quad (3)$$

The surface response function $g(\overline{q}, \omega)$ is a key quantity that determines how the solid interacts with the environment. Some well-known examples in which it plays a relevant role are heat transfer [39], non-contact friction [40], molecule vibration damping [41], etc.

We calculate $\chi(z, z', \overline{q}, \omega)$ in terms of the density response function for non-interacting electrons $\chi^o(z, z', \overline{q}, \omega)$ using the random phase approximation:

$$\chi(z,z',\overline{q},\omega) = \chi^o(z,z',\overline{q},\omega) + \int \mathrm{d}z_1\int \mathrm{d}z_2\,\chi^o(z,z_1,\overline{q},\omega)\frac{2\pi\,\mathrm{e}^{-\overline{q}|z_1-z_2|}}{\overline{q}} \times \chi(z_2,z',\overline{q},\omega) \quad (4)$$

with

$$\chi^o(z,z',\overline{q},\omega) = 2\sum_{i,j}\varphi_i(z)\varphi_j^*(z)\varphi_j(z')\varphi_i^*(z') \times \int \frac{\mathrm{d}\overline{\mathbf{k}}}{(2\pi)^2}\frac{\theta(E_\mathrm{F}-E_i)-\theta(E_\mathrm{F}-E_j)}{E_i-E_j+(\omega+\mathrm{i}\eta)}, \quad (5)$$

where $\eta$ is a positive infinitesimal that in the present calculations was chosen to be 1 meV, $E_i = \varepsilon_i + \overline{\mathbf{k}}^2/(2m_i)$, $E_j = \varepsilon_j + (\overline{\mathbf{k}}+\overline{\mathbf{q}})^2/(2m_j)$, and $E_\mathrm{F}$ is the Fermi energy of the system. Here, the energies $\varepsilon_i$ and wavefunctions $\varphi_i$ are the solutions of the one-dimensional Schrödinger equation that describes the system along the surface normal. The effective masses $m_i$ and $m_j$ associated with the surface state and bulk electrons have been taken to reproduce the realistic surface band structure of the metal. The sums over $i$ and $j$ include both occupied and unoccupied electronic states. Some authors [23, 42] evaluate $\chi$ and $\chi^o$ in real space. Here we adopt an approach based on the calculation of these quantities in reciprocal space [24, 25]. Further calculation details of the procedure followed to evaluate $\chi$ can be found in [43]. In order to characterize the noble metal surfaces, we obtain $\varepsilon_i$ and $\varphi_i$ by solving the Schrödinger equation with the use of the one-dimensional model potential for the Cu(111), Ag(111), and Au(111) surfaces reported in [32]. Each potential is constructed to reproduce the key ingredients of the surface electronic structure, namely the width and position of the energy gap at the center of the surface Brillouin zone and the energy positions of both the surface and first image states.

## 3. Calculation results

From equation (2) one can see that the stopping power $S(b)$ of a charged particle traveling in front of a metal surface is determined by the imaginary part of the surface response function, a key ingredient of the present calculations. Due to the presence of the exponential term in the integrand of equation (2), the dependence of $S(b)$ on $b$ at large distances from the surface is determined by details of the surface loss function $\mathrm{Im}[g(\overline{q}, \omega)]$ at small $\overline{q}$. Moreover, for low projectile velocities only the magnitude of $\mathrm{Im}[g(\overline{q}, \omega)]$ at small energies plays a role (see integration limits in equation (2)). The properties of $\mathrm{Im}[g(\overline{q}, \omega)]$ were intensively investigated in the past with the jellium model [41]. In particular, it was demonstrated that $\mathrm{Im}[g(\overline{q}, \omega)]$ for small $\overline{q}$ and small $\omega$ is proportional to $\overline{q}$ and $\omega$. Nevertheless, as shown in figures 3–5, the surface loss function $\mathrm{Im}[g(\overline{q}, \omega)]$ of Cu(111), Ag(111), and Au(111), is strongly inhomogeneous when the realistic band structure, with a partially occupied surface state, is incorporated in the model. Furthermore, the surface loss function is dominated by the regions labeled as '2D + 3D' which correspond to electron–hole pair excitations in the surface state. Hence, for small $\overline{q}$ and $\omega$, $\mathrm{Im}[g(\overline{q}, \omega)]$ is no longer proportional to $\overline{q}$. Additionally, the presence of an acoustic surface plasmon [34, 44] at small $\overline{q}$ and $\omega$ (shown by a solid line in figures 3–5) leads to a strong peak structure in $\mathrm{Im}[g(\overline{q}, \omega)]$ as seen in figure 6. In figure 6 for comparison we also show $\mathrm{Im}[g(\overline{q}, \omega)]$ obtained within the jellium model for a mean electron radius $r_s = 2.67$ a.u., which accounts for the valence band electrons in copper. In the jellium model, $\mathrm{Im}[g(\overline{q}, \omega)]$ has a featureless behavior in this $(\overline{q} - \omega)$ domain, in striking contrast to the realistic Cu(111) case. The left and right borders of the '2D + 3D'areas in figures 3–5, are determined by the binding energy, $E_\mathrm{F}^{\mathrm{SS}}$, and effective mass, $m_{\mathrm{SS}}^*$, of the corresponding surface state as $\omega = \upsilon_\mathrm{F}^{\mathrm{SS}}\overline{q} + \overline{q}^2/2m_{\mathrm{SS}}^*$ and $\omega = -\upsilon_\mathrm{F}^{\mathrm{SS}}\overline{q} + \overline{q}^2/2m_{\mathrm{SS}}^*$, respectively. Here $\upsilon_\mathrm{F}^{\mathrm{SS}}$ is the surface state Fermi velocity. For the surfaces under study, we use experimentally determined values of $E_\mathrm{F}^{\mathrm{SS}}$ and $m_{\mathrm{SS}}^*$. For Cu(111), Ag(111), and Au(111) they are 0.44 eV and 0.42, 0.067 eV and 0.44, and 0.47 eV and 0.28, respectively. This difference in the surface state characteristics for these surfaces is reflected in the different size of the '2D + 3D'

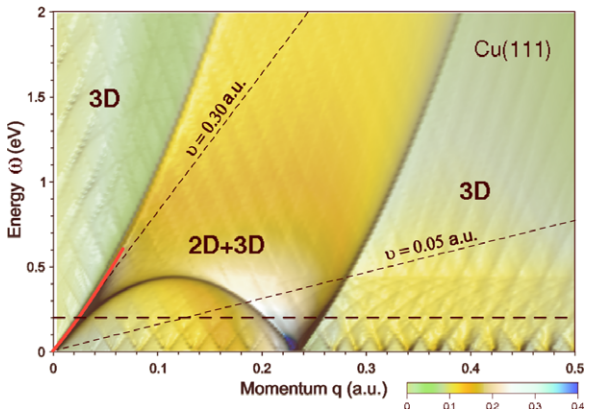


**Figure 3.** False-color plot of the normalized surface loss function $\mathrm{Im}[g(\overline{q},\omega)]/\omega$ for the Cu(111) surface versus the two-dimensional momentum $\overline{q}$ and energy $\omega$. The phase-space regions where only bulk intra-band electron–hole pair excitations are permitted are denoted by '3D'. The region where the intra-band electron–hole excitations within the surface state are additionally possible is denoted by '2D + 3D'. The thick solid line represents dispersion of an acoustic surface plasmon [34]. Two thin dashed lines limit the upper borders of the phase-space regions where the excitations can be produced by the moving charged particle with velocity $\upsilon = 0.05$ a.u. and 0.3 a.u., respectively. The horizontal long dashed line shows the cut along which $\mathrm{Im}[g(\overline{q},\omega)]$ is displayed in figure 6.

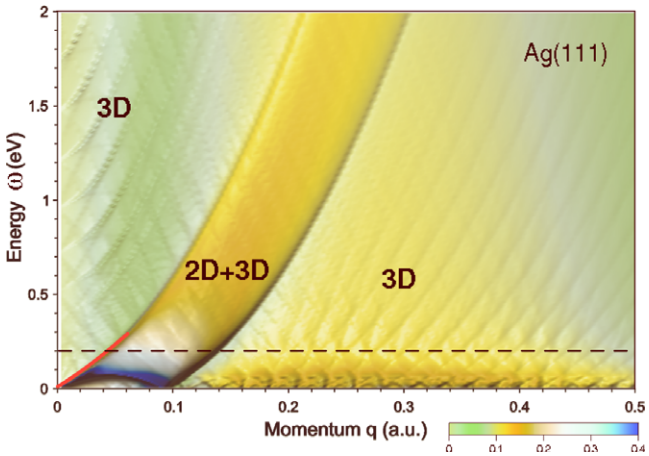


**Figure 4.** False-color plot of the normalized surface loss function $\mathrm{Im}[g(\overline{q},\omega)]/\omega$ for the Ag(111) surface versus the two-dimensional momentum $\overline{q}$ and energy $\omega$. The phase-space regions where only bulk intra-band electron–hole pair excitations are permitted are denoted by '3D'. The region where the intra-band electron–hole excitations within the surface state are additionally possible is denoted by '2D + 3D'. The thick solid line represents dispersion of an acoustic surface plasmon [34]. The horizontal long dashed line corresponds to the cut along which $\mathrm{Im}[g(\overline{q},\omega)]$ is presented in figure 6.

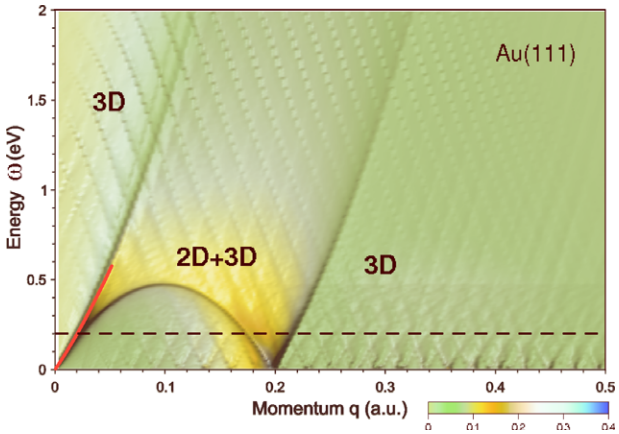


**Figure 5.** False-color plot of the normalized surface loss function $\mathrm{Im}[g(\overline{q},\omega)]/\omega$ for the Au(111) surface versus the two-dimensional momentum $\overline{q}$ and energy $\omega$. The phase-space regions where only bulk intra-band electron–hole pair excitations are permitted are denoted by '3D'. The region where the intra-band electron–hole excitations within the surface state are additionally possible is denoted by '2D + 3D'. The thick solid line represents dispersion of an acoustic surface plasmon [34]. The horizontal long dashed line corresponds to the cut along which $\mathrm{Im}[g(\overline{q},\omega)]$ is presented in figure 6.

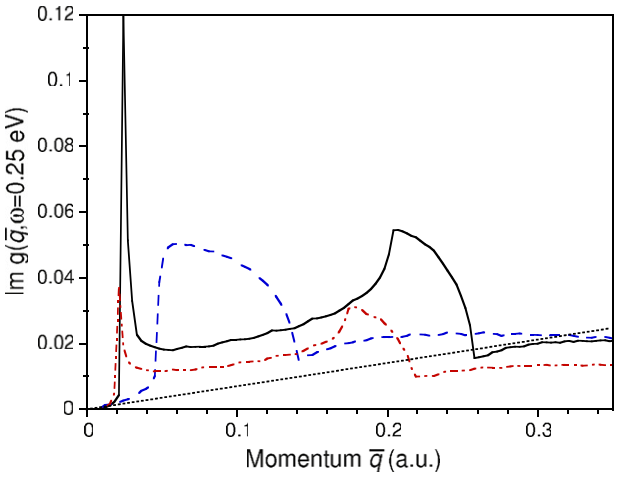


**Figure 6.** Surface loss function $\mathrm{Im}[g(\overline{q},\omega)]$ versus the two-dimensional momentum $\overline{q}$ for $\omega = 0.25$ eV (corresponds to the cut along the horizontal long dashed line in figures 3–5). Solid, dashed, and dashed–dotted lines stand for Cu(111), Ag(111), and Au(111), respectively. The dotted line shows $\mathrm{Im}[g(\overline{q},\omega)]$ calculated within a jellium model with $r_s = 2.67$ usually employed for description of a Cu metal.

areas. It is maximal for Cu(111) and minimal for Ag(111). On the contrary, comparison between figures 3–6 reveals that the amplitude of $\mathrm{Im}[g(\overline{q},\omega)]$ follows another trend—it is maximum for Ag(111) and significantly reduced at the Au(111) surface.

All these facts strongly modify the asymptotic behavior of $\gamma(b,\upsilon)$ and $S(b,\upsilon)$ (presented in figures 7, 8, and 9 for Cu(111), Ag(111), and Au(111), respectively) at large distances from the surface in comparison with the one expected from the jellium model [23, 42]. Figures 7–9 demonstrate clearly the non-monotonic behavior of $\gamma(b,\upsilon)$ and $S(b,\upsilon)$ with the distance $b$ and velocity $\upsilon$. Thus at small $b$ the stopping power (friction coefficient), which is governed by the electron–hole excitations in the bulk electronic system, increases almost linearly (constant) with increasing projectile velocity, similarly to results derived within the jellium model. As the distance increases, the situation changes. In this case the relative role

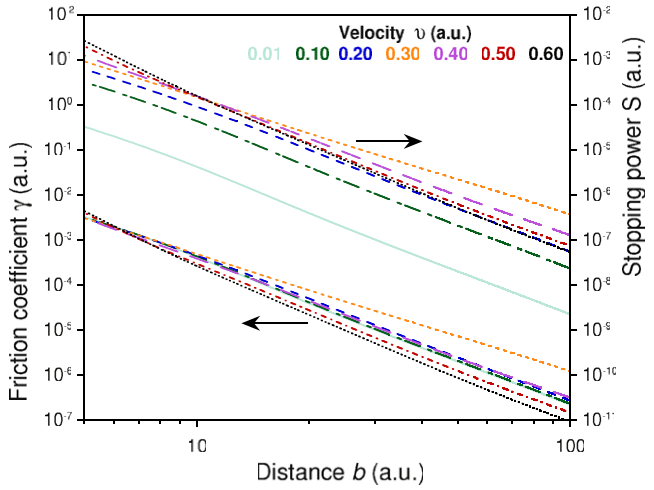


**Figure 7.** Friction coefficient $\gamma(b, \upsilon)$ (left) and stopping power $S(b, \upsilon)$ (right) for a projectile of charge $Z_1 = 1$ moving parallel to the Cu(111) surface versus its distance $b$ from the surface for some values of velocity $\upsilon$. Solid, long dashed–dashed, dashed, short dashed, long dashed, dashed–dotted, dotted lines stand for $\upsilon = 0.01$, 0.1, 0.2, 0.3, 0.4, 0.5, 0.6 a.u., respectively.

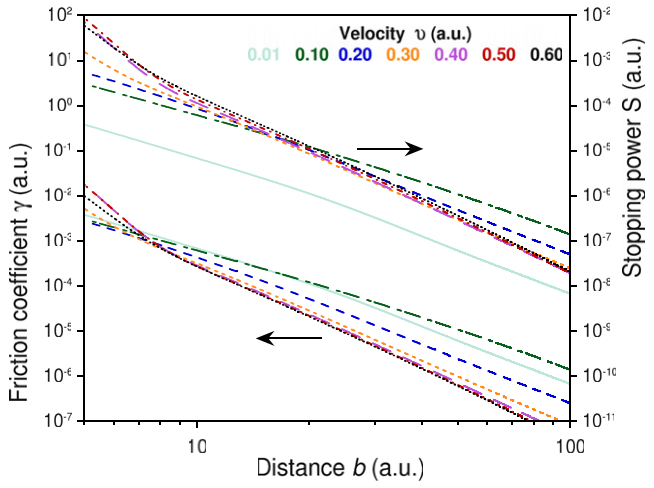


**Figure 8.** Friction coefficient $\gamma(b, \upsilon)$ (left) and stopping power $S(b, \upsilon)$ (right) for a projectile of charge $Z_1 = 1$ moving parallel to the Ag(111) surface versus its distance $b$ from the surface for some values of velocity $\upsilon$. Solid, long dashed–dashed, dashed, short dashed, long dashed, dashed–dotted, dotted lines stand for $\upsilon = 0.01$, 0.1, 0.2, 0.3, 0.4, 0.5, 0.6 a.u., respectively.

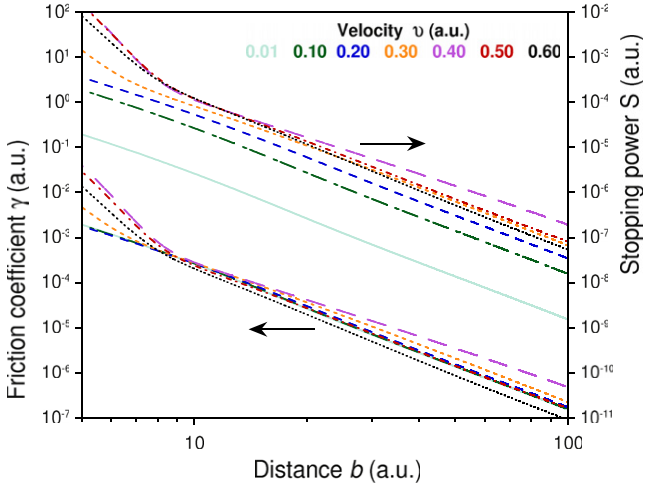


**Figure 9.** Friction coefficient $\gamma(b, \upsilon)$ (left) and stopping power $S(b, \upsilon)$ (right) for a projectile of charge $Z_1 = 1$ moving parallel to the Au(111) surface versus its distance $b$ from the surface for some values of velocity $\upsilon$. Solid, long dashed–dashed, dashed, short dashed, long dashed, dashed–dotted, dotted lines stand for $\upsilon = 0.01$, 0.1, 0.2, 0.3, 0.4, 0.5, 0.6 a.u., respectively.

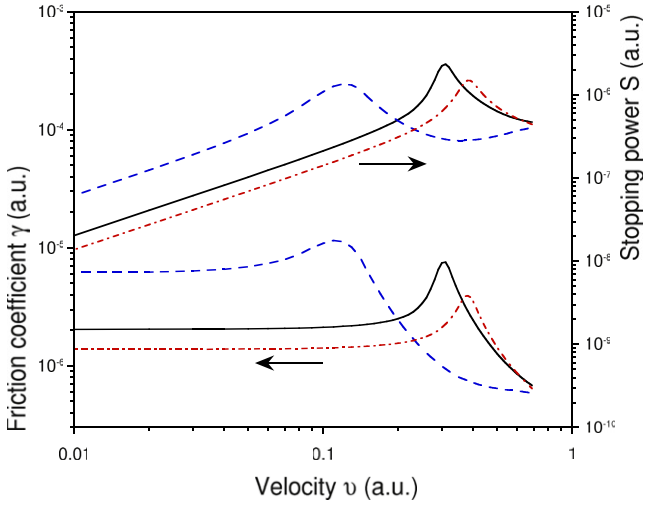


**Figure 10.** Friction coefficient $\gamma(b, \upsilon)$ (left) and stopping power $S(b, \upsilon)$ (right) for a projectile of charge $Z_1 = 1$ moving parallel to the (111) surface of Cu (solid lines), Ag (dashed lines), and Au (dashed–dotted lines) at the distance $b = 50$ a.u. versus projectile velocity $\upsilon$.

of excitations involving the surface state starts gradually to be more important. Thus, for small velocities it leads to the $\sim b^{-3}$ dependence of $\gamma(b, \upsilon)$ and $S(b, \upsilon)$ on distance $b$ due to electron–hole production within the surface state [31] instead of the $\sim b^{-4}$ law expected from the jellium model [10, 41].

In figure 10 we plot the friction coefficient and stopping power for all three systems as a function of projectile velocity at the distance $b = 50$ a.u. In the figure, it is clearly seen that there is some threshold velocity at which an additional energy loss channel arises. For all three surfaces the value of this threshold velocity is different. As the velocity increases further, $\gamma(\upsilon)$ and $S(\upsilon)$ reach a maximum and drop down for higher $\upsilon$. Careful analysis of different constituents in the integral of equation (2) reveals that this remarkable behavior is a consequence of the presence in $\mathrm{Im}[g(\overline{q}, \omega)]$ of a strong peak due to the acoustic surface plasmon existing in these surfaces (see figures 3–5). Additionally, the quasi-linear sound-like dispersion of the acoustic plasmon at small $\overline{q}$ leads to a distance-decay of $\gamma(b)$ and $S(b)$ for projectile velocities close to the surface state Fermi velocity, significantly slower than the mentioned decay of $\sim b^{-3}$. The surface state Fermi velocities for the Cu(111), Ag(111), and Au(111) systems are $\upsilon_{\mathrm{F}}^{\mathrm{SS}} = 0.28$, 0.11, and 0.35 a.u., respectively. In this case the decay is fitted by the $\sim b^{-2}$ law. The origin of this is the above-mentioned sound-like acoustic surface plasmon dispersion and

the presence of the pole divergency in equation (2) in the vicinity of the upper limit of the integral on $\omega$. Hence the main contribution to the integral comes from the region where $\omega \approx \overline{q}v$. When the projectile velocity $v$ is close to the group velocity of the acoustic surface plasmon (which almost coincides with the surface state Fermi velocity [45]) a strong increase of $\gamma(b, v)$ and $S(b, v)$ is observed. The subsequent decrease of the friction coefficient and stopping power for projectile velocities larger than $v_F^{SS}$ is explained by the fact that the main contribution to the integral of equation (2) comes in this case from the $\overline{q} - \omega$ region where $\mathrm{Im}[g(\overline{q}, \omega)]$ is determined by the bulk electron–hole excitations (the left '3D' regions in figures 3–5) and which is significantly smaller than in the '2D + 3D' phase-space region.

Note that this peak-structure behavior of the friction coefficient and stopping power can be severely affected by excitations involving electrons from the occupied valence d band [30, 46–48]. In the case of gold, the threshold for this channel is somewhat lower than the threshold for acoustic surface plasmon excitation. Nevertheless, in the low-momentum limit these excitations cannot be produced by the slow projectile. Hence, the asymptotic behavior of the friction coefficient and stopping power should be correctly represented by the present model.

We are not aware of any experiment which could be used to test our findings. The problem with grazing scattering of ions with surfaces is that in this kind of experiment the ions are usually reflected close to the topmost layer of atoms where the electronic density is high and most of the energy loss takes place. From figures 7–9 it is clear that in order to observe the predicted energy loss peak related to the excitations of the acoustic surface plasmon, it is necessary to probe the projectile surface distances longer than 5 a.u. The reason is that one needs to avoid trajectories close to the surface, since for these trajectories the predicted effect is masked by the energy loss mechanism that takes place at short distances. In this respect, analysis of the energy loss of ions traveling through microcapillaries could be a good way to test our predictions. Through microcapillaries the ions can cruise over large distances ($\geqslant 1$ $\mu$m) parallel to the surface at distances around and below 100 nm. Therefore, in principle, it is possible to probe energy losses at the necessary microscopically large distances [23].

## 4. Conclusions

We have studied the stopping power, $S$, and friction coefficient, $\gamma$, for a charged particle traveling parallel to the Cu(111), Ag(111), Au(111) surfaces. We demonstrate that for large distances and projectile velocities lower than the Fermi velocity of the partly occupied quasi-two-dimensional s–$p_z$ surface state, $S$ and $\gamma$ are dominated by electron–hole excitations within the surface state. $S$ and $\gamma$ decrease with increasing distance $b$ from the surface with characteristic $\sim b^{-3}$ decay instead of the $\sim b^{-4}$ behavior expected from the jellium and other simple models. Additionally we show that $S$ and $\gamma$ behave non-monotonically with increasing velocity and reach maximum values at $v$ close to the surface state Fermi velocity $v_F^{SS}$. At such velocities, the dominant contributions to $S$ and $\gamma$ come from the excitation of the acoustic surface plasmon and its decay with distance $b$ obeys a characteristic $\sim b^{-2}$ law. This behavior of $S$ and $\gamma$ versus $v$ and $b$ is related to the strongly non-monotonic behavior of the surface loss function at small $\omega$ and $\overline{q}$ for these surfaces which is governed by electron–hole excitations within the surface state band and the acoustic surface plasmon.

## Acknowledgments

This work has been partially funded by the University of the Basque Country UPV/EHU (Grant No. 9/UPV 00206.215-13639/2001), the Eusko Jaurlaritza, and the Spanish MCyT (Grant No. FIS2007-066711-CO2-00).

## References

[1] Winter H 2002 *Phys. Rep.* **367** 387
[2] Kimura K, Hasegawa M and Mannami M 1987 *Phys. Rev.* B **36** 7
[3] Wilke M, Zimny R and Winter H 1995 *Nucl. Instrum. Methods Phys. Res.* B **100** 396
[4] Winter H, Wilke M and Bergomaz M 1997 *Nucl. Instrum. Methods Phys. Res.* B **125** 124
[5] Juaristi J I, Arnau A, Echenique P M, Auth C and Winter H 1999 *Phys. Rev. Lett.* **82** 1048
[6] Juaristi J I, Arnau A, Echenique P M, Auth C and Winter H 1999 *Nucl. Instrum. Methods Phys. Res.* B **157** 87
[7] Robin A, Heiland W, Jensen J, Juaristi J I and Arnau A 2001 *Phys. Rev.* A **64** 052901
[8] Echenique P M and Pendry J B 1975 *J. Phys. C: Solid State Phys.* **8** 2936
[9] Ferrell T L and Echenique P M 1985 *Phys. Rev. Lett.* **55** 1526
[10] Nuñez R, Echenique P M and Ritchie R H 1980 *J. Phys. C: Solid State Phys.* **13** 4229
[11] Zabala N and Echenique P M 1990 *Ultramicroscopy* **32** 327
[12] Juaristi J I and García de Abajo F J 1994 *Nucl. Instrum. Methods Phys. Res.* B **90** 252
[13] Juaristi J I, García de Abajo F J and Echenique P M 1996 *Phys. Rev.* B **53** 13839
[14] Song Y-H and Wang Y-N 1999 *Nucl. Instrum. Methods Phys. Res.* B **153** 186
[15] Song Y-H, Wang Y-N and Mišković Z L 2001 *Phys. Rev.* A **63** 052902
[16] Ritchie R H and Marusak A L 1966 *Surf. Sci.* **4** 234
[17] Wagner D 1966 *Z. Naturf.* A **21** 634
[18] Gravielle M S 1998 *Phys. Rev.* A **58** 4622
[19] Gravielle M S and Miraglia J E 2002 *Phys. Rev.* A **65** 022901
[20] Cazalilla M A and García de Abajo F J 1997 *Nucl. Instrum. Methods Phys. Res.* B **125** 106
[21] Cazalilla M A and Juaristi J I 1999 *Nucl. Instrum. Methods Phys. Res.* B **157** 104
[22] García-Lekue A and Pitarke J M 2001 *Phys. Rev.* B **64** 035423
[23] Tökési K, Tong X M, Lemell C and Burgdörfer J 2005 *Phys. Rev.* A **72** 022901
[24] Eguiluz A G 1983 *Phys. Rev. Lett.* **51** 1907
[25] Eguiluz A G 1985 *Phys. Rev.* B **31** 3303
[26] Zangwill A and Soven P 1980 *Phys. Rev.* A **21** 1561
[27] Alducin M, Silkin V M, Juaristi J I and Chulkov E V 2002 *Nucl. Instrum. Methods Phys. Res.* B **193** 585
[28] Alducin M, Silkin V M, Juaristi J I and Chulkov E V 2003 *Phys. Rev.* A **67** 032903
[29] Faraggi M N, Gravielle M S, Alducin M, Juaristi J I and Silkin V M 2005 *Phys. Rev.* A **72** 012901

[30] Gravielle M S, Alducin M, Juaristi J I and Silkin V M 2007 *Phys. Rev.* A **76** 044901
[31] Alducin M, Silkin V M and Juaristi J I 2007 *Nucl. Instrum. Methods Phys. Res.* B **256** 383
[32] Chulkov E V, Silkin V M and Echenique P M 1999 *Surf. Sci.* **437** 330
[33] Chulkov E V, Silkin V M and Echenique P M 1997 *Surf. Sci.* **391** L1217
[34] Silkin V M, García-Lekue A, Pitarke J M, Chulkov E V, Zaremba E and Echenique P M 2004 *Europhys. Lett.* **66** 260
[35] Gartland P O and Slagsvold B J 1975 *Phys. Rev.* B **12** 4047
[36] Kevan S D (ed) 1992 *Angle-resolved Photoemission Studies in Surface Science and Catalysis* vol 74 (Amsterdam: Elsevier)
[37] Hüfner S 1995 *Photoelectron Spectroscopy—Principles and Applications* (*Springer Series in Solid-State Science* vol 74) (Berlin: Springer)
[38] Persson B N J and Zaremba E 1985 *Phys. Rev.* B **31** 1863
[39] Pendry J B 1997 *J. Phys.: Condens. Matter* **9** 10301
[40] Volokitin A I and Persson B N J 2007 *Rev. Mod. Phys.* **79** 1291
[41] Liebsch A 1997 *Electronic Excitations at Metal Surfaces* (New York: Plenum)
[42] Liebsch A 1997 *Phys. Rev.* B **55** 13263
[43] Silkin V M, Pitarke J M, Chulkov E V and Echenique P M 2005 *Phys. Rev.* B **72** 115435
[44] Diaconescu B, Pohl K, Vattuone L, Savio L, Hofmann P, Silkin V M, Pitarke J M, Chulkov E V, Echenique P M, Farias D and Rocca M 2007 *Nature* **448** 57
[45] Pitarke J M, Nazarov V U, Silkin V M, Chulkov E V, Zaremba E and Echenique P M 2004 *Phys. Rev.* B **70** 205403
[46] Valdés J E, Eckardt J C, Lantschner G H and Arista N R 1994 *Phys. Rev.* A **49** 1083
[47] Chenakin S P, Markin S N, Steinbauer E, Draxler M and Bauer P 2006 *Nucl. Instrum. Methods Phys. Res.* B **249** 58
[48] Figueroa E A, Cantero E D, Eckardt J C, Lantschner G H, Valdés J E and Arista N R 2007 *Phys. Rev.* A **75** 010901(R)